Available online at www.sciencedirect.com
ScienceDirect
Journal of the European Ceramic Society 29 (2009) 677–689
www.elsevier.com/locate/jeurceramsoc

A nanophase oxygen storage material: Alumina-coated metal-based ceria

Othon Adamopoulos [a,*], Eva Björkman [a], Yu Zhang [a], Mamoun Muhammed [a], Tassilo Bog [b], Lothar Mussmann [b], Egbert Lox [b]

[a] *Functional Materials Division, Nano Characterisation Centre, Department of Microelectronics and Applied Physics, The Royal Institute of Technology, S-164 40 Stockholm, Sweden*
[b] *Umicore AG & Co. KG, PO Box 1351, D-63403 Hanau, Germany*

Received 20 December 2007; received in revised form 2 July 2008; accepted 11 July 2008
Available online 5 September 2008

Abstract

Nanoparticles of $Ce_{1-x}M_xO_{2-\delta}$ (M = Ca or Zr) coated with Al_2O_3 with average crystallite size of 10 nm have been synthesised via solution chemistry approach under controlled chemical and hydrodynamic conditions. Their synthesis has been accomplished in three major steps: (1) simultaneous co-precipitation of cations, (2) sequential precipitation of $Al(OH)_3$ over the former particles and (3) calcination of the precipitated precursors to the corresponding oxides. Several compositions have been synthesised and their physicochemical properties are compared with commercial state-of-the-art material. The Al_2O_3-coating hinders the particles growth at high temperatures, resulting in materials with a large specific surface area and a restrain in the decrease of their oxygen storage capacity.

Keywords: Calcination; Composites; Nanocomposites; CeO_2; Grain size

1. Introduction

Nanosized materials have a very high specific surface area[1,2] and thus the relative amount of structural defects on the surface of their particles is increased. That can explain the enhanced redox activity of these particles in the preceding article of this series.[3] Cerium dioxide – CeO_2 or ceria – has been extensively used in Three-Way automobile Catalysts (TWC) and for solid oxide fuel cells applications because of its good conductivity of oxygen ions. The function of this material is mainly based on its ability to oscillate between Ce(III) and Ce(IV) oxidation states upon changes in redox conditions.[4,5] This process is reversible, thereby rendering ceria, CeO_2, suitable for oxygen storage. Oxygen Storage Capacity (OSC) of CeO_2 enables the automobile catalytic converter to operate more efficiently, by making the catalyst less sensitive to variations of O_2 concentration that occur in the exhaust stream under normal driving conditions.

Upon its extended use, a TWC tends to deteriorate its conversion efficiency because the OSC of its CeO_2 support declines. A possible cause for such an aging effect is the growth of CeO_2 particles when used at high temperature or for a long time, which results in a decrease of the active surface area. Therefore, there is a need for developing thermally more stable materials for oxygen storage, which can withstand high temperatures for longer period.

One approach to thermally stabilise the catalyst is to use alumina, Al_2O_3, since it is known to be heat-resistant and thermally stable in both oxidising and reducing atmospheres up to approximately 2000 °C.[6] Furthermore, Al_2O_3 is resistant to various chemical attacks, and so used in many applications, such as refractory lining, spark plugs, missile nose cones and pumps. Alumina appears in several crystalline forms, of which the α-phase is the most stable and dense.[7] Another thermally stable material is zirconia, ZrO_2, which has come into widespread uses recently. The combination of good thermal insulation, chemical inertness and high thermal stability are few among the many features of ZrO_2 that have made various forms of it attractive for a wide range of applications.

The Ce/Zr/Al based-oxides have been shown to possess an increased thermal stability and capacity for hydrogen

* Corresponding author.
E-mail address: othona@kth.se (O. Adamopoulos).

0955-2219/$ – see front matter © 2008 Elsevier Ltd. All rights reserved.
doi:10.1016/j.jeurceramsoc.2008.07.017

absorption at elevated temperatures.[8] Several methods have been described for the synthesis of doped cerium oxides, such as co-precipitation,[3,7,9,10] high-temperature firing,[11] high-energy milling of the mixture oxides[12] and sol–gel methods.[13] The co-precipitation method demonstrates the advantage to allow the mixing of different elements at the atomic level, since the starting compounds are completely dissolved in liquid solutions. Therefore, this method is highly advantageous when multi-component oxides are to be synthesised. Besides, with thermodynamic modelling it is feasible to design suitable operating conditions, under which all of the components can be co-precipitated at the required stoichiometry. The resulting powder – either a composite, a solid solution or even a mixture of several compounds – can be in a highly homogenous form even at the sub-micrometer level.

In preceding papers the synthesis of nanophase doped CeO_2 via the co-precipitation method using oxalates has been reported.[3,7,14,15] The method has been used to synthesise several samples of CeO_2 doped with a variety of cations – e.g. Ba, Ca, Co, Zn and Zr – forming solid solutions. Most of these materials showed enhancement of both OSC and redox activities compared to undoped CeO_2.[3,7,16,17] In another study the synthesis of Ce–Zr–Al based-oxides, along with other cations, has been performed, where co-precipitation of the corresponding compounds has taken place under alkaline solution.[18,19] Ceria powders synthesised by co-precipitation were also mixed with Al_2O_3 to improve the specific surface area and resist the particles growth of CeO_2 at the elevated temperatures where the catalytic converters operate.[20] However, the concept of sequential precipitation of Al_2O_3-coating over the Ce–Zr or Ce–Ca particles has not been reported earlier.

In the present study,[21] the synthesis of Al_2O_3-coated nanosized powders of the Ce–Zr and Ce–Ca systems is introduced and their OSC and physicochemical properties are investigated.

2. Experimental procedure

2.1. Synthesis principles

The synthesis of the Al_2O_3-coated nanoparticles of $Ce_{1-x}M_xO_{2-\delta}$ (M = Ca or Zr) has been accomplished in three major parts. Particularly, in the case of the Ce/Ca system, the synthesis of $Ce_{0.9}Ca_{0.1}O_{2-\delta}{\cdot}0.5Al_2O_3$ sample has been carried out in two different procedures. In the former, the sample was synthesised by the simultaneous co-precipitation of $Ce_2(C_2O_4)_3$, $CaCO_4$ and $Al(OH)_3$ under controlled hydrodynamic, i.e. mixing, and chemical, i.e. pH conditions (cf. Fig. 1(a)). In the latter, Ce–Ca–oxalate co-precipitated at first simultaneously, to be then followed by the precipitation of $Al(OH)_3$. In this case, the Ce–Ca–oxalate particles served as seeds, on which $Al(OH)_3$ precipitated subsequently, thereby forming a coat over the surface of Ce–Ca–oxalate (cf. Fig. 1(b)).

The kinetics of the precipitation of Zr(IV) with oxalate $(C_2O_4)^{2-}$ is quite slow and the solubility of $Zr_2(C_2O_4)_4$ is relatively high, resulting in uncontrollable composition.[15] To circumvent that roadblock, Zr(IV) was precipitated as ZrO_2 under controlled conditions. Thus, in the case of the Ce/Zr system, the oxalate $(C_2O_4)^{2-}$ amount mixed with the metals solution was stoichiometrically calculated for Ce(III) only and not for Zr(IV), so as to simultaneously precipitate as $Ce_2(C_2O_4)_3$ and ZrO_2, respectively. Subsequently, $Al(OH)_3$ precipitated over the surface of the already formed Ce–Zr particles, thereby forming a coat. Afterwards, the co-precipitated powders of both Ce–Zr and Ce–Ca systems were dried and heat treated at appropriate temperatures to form the corresponding oxides.

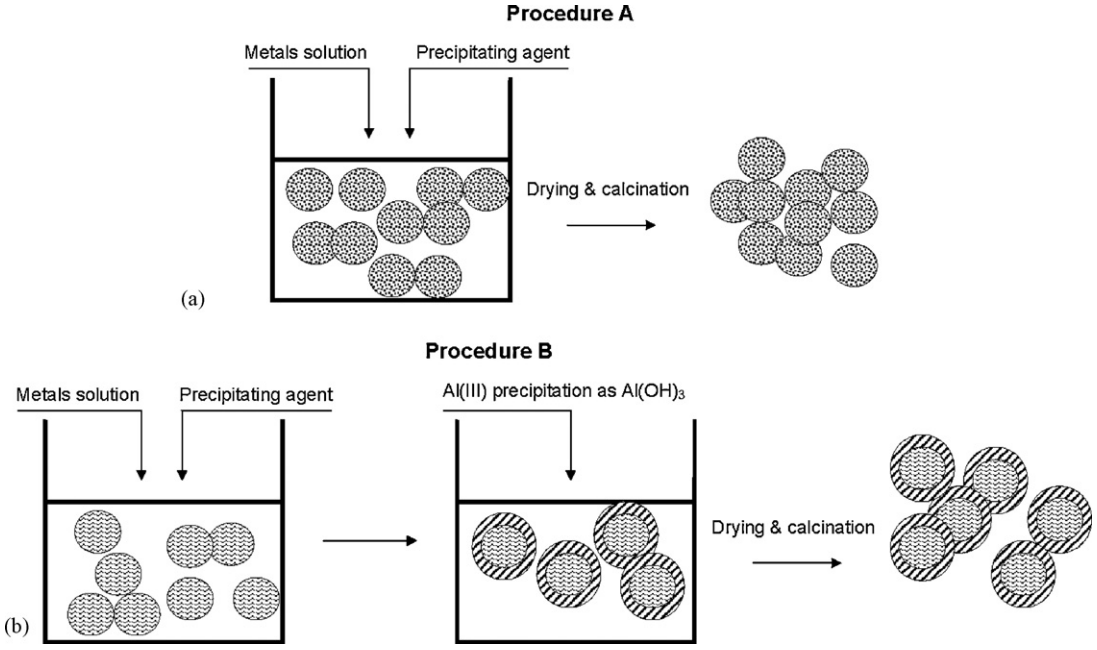

Fig. 1. The principles of (a) the simultaneous co-precipitation and (b) the sequential precipitation of Al(III) coating process.

2.1.1. Thermodynamic modelling

A significant step was to identify the optimum conditions for the simultaneous precipitation of the different cations, i.e. Ca(II), Ce(III), Zr(IV) or Al(III). Computer software for modelling of the chemical equilibrium, developed at 'The Royal Institute of Technology', was used to assist in identifying these conditions. This program, 'Medusa',[22] uses solubility products and formation constants of soluble complexes. Details of the modelling approach have been published elsewhere.[23,24] Suitable conditions, e.g. pH, cation and anion concentrations, and sequence of mixing are obtained using this software.

2.1.2. Nomenclature

To simplify the way of presenting the chemical composition of the samples, a nomenclature/identification has been addressed. The number next to each element denotes the chemical composition (i.e. molar %) of its oxide, e.g. Ce80Zr20 means that this compound consists of 80% CeO_2 and 20% ZrO_2 molar composition. The abbreviations – or combination of them – in parenthesis denote the followings: (lit) literature, (ppt) precipitation, (p) precursor, (a) aged material, (seq) sequential, (sim) simultaneous, (comm) commercial, (b) small volume synthesis reactor, i.e. beaker, (r) large volume synthesis reactor (cf. Table 1).

2.1.3. Synthesis

The synthesis was performed both in a laboratory reactor of small volume and in a larger volume (3.2 L), special, automatically controlled, home-made reactor. [21] Solutions, containing mixtures of the metal cations Ce(III) and Zr(IV) or Ca(II) were simultaneously mixed with the oxalate-containing solution and/or $Al(OH)_3$ under automatically controlled flow rates with the aid of peristaltic pumps. The addition of the solutions was accomplished at a rate of 5 ml min^{-1} into the synthesis reactor, under vigorous mechanical stirring at a suitable constant pH, at which the co-precipitates were formed. The respective range of these pH values for each sample is included in Table 2. The precipitates were stirred in the synthesis reactor for max 30 min after the mixing of the solutions was terminated, or before Al(III) was added. In the case of the sequential precipitation of Al(III), its addition was accomplished at a rate of 5 ml min^{-1}, as well.

After the addition of all solutions, the precipitate was filtered off using water pump and rinsed with deionised H_2O to remove any residual mother-liquor. The synthesised powders were dried in air at 105 °C overnight, and then the temperature was increased to 400 °C with rapid heating rate (ca. 10 °C min^{-1}) for 2 h. Some samples of the Ce–Ca system were also calcined at 600 °C for 3 h. All these samples are hereinafter called as calcined materials. Afterwards the samples were cooled down to room temperature. Most of the samples were further heat treated up to 650 °C in air with the same heating rate for additional 4 h. These samples are hereinafter called as aged materials.

2.2. Chemicals and solutions

The solutions of the metal components were prepared from their corresponding nitrate salts – e.g. $Ce(NO_3)_3{\cdot}6H_2O$ (Chempur), $Ca(NO_3)_2{\cdot}4H_2O$ and $Al(NO_3)_3$ (Merck). Moreover, $Zr(NO_3)_4$ solution with concentration of 30 wt% ZrO_2, powders of CeO_2 and ZrO_2 (Kebo AB, Sweden) were used as received. Diluted solutions of NH_4OH and HNO_3 were used for the pH adjustment. A sample of commercial state-of-the-art high-surface Ce/Zr oxide, containing 30 wt% ZrO_2 and 70 wt% CeO_2, was used for comparison.

2.3. Analysis and characterisation

2.3.1. Chemical analysis

The Ca(II) and Al(III) concentrations of the filtrate, precursor or calcined materials were determined by Atomic Absorption Spectrophotometry (AAS) SpectrAA-200, Varian. Further chemical analysis of the samples was performed by the Energy Dispersive Spectroscopy (EDS) of the Scanning Electron Microscopy (SEM, JEOL JSM-880).

2.3.2. Thermogravimetric analysis

The decomposition process and the weight loss of the precursor materials as a function of the temperature were recorded under flow O_2(g)–N_2(g) by thermogravimetric analysis apparatus (Thermogravimetric Analyser, TGA 7, PerkinElmer Instr. Inc.) with a heating rate of 10° C min^{-1}.

2.3.3. Phase identification

X-ray Diffraction (XRD) was performed with a monochromatised X-ray beam with the nickel-filtered Cu Kα radiation (λ = 1.5418 Å), to study the phase crystallinity, identification and constituents of the powders (Philips PW 1012/20). The data was compared to reference data from the International Centre for Diffraction Data (ICDD). Spectra were taken from $2\theta = 5$–$75°$, with a 0.05° step size and a counting time of 0.5 s. Powder of Si (Riedel-de Haēn) has been used for the calibration of the X-ray diffractometer. The lattice parameter (α) of the cubic structure of the CeO_2 phase was calculated based on the (*hkl*) indices of its main peaks (2θ), i.e. (1 1 1), (2 2 0), (3 1 1) and (2 0 0), as shown in Fig. 2. The average crystalline diameter (D) is obtained from the Scherrer equation.[25,26]

2.3.4. Specific surface area and density measurements

The specific surface area, S_{BET}, of the samples was analysed under N_2(g) (Gemini 2370 Surface Area Analyzer). Prior to the measurements, the samples were outgassed at 110 °C overnight. Additionally, pycnometer (AccuPyc 1330, Micromeritics, Norcross – GA 30093-1877) was used for the determination of the samples density (ρ) under He(g).

2.3.5. Particles size measurements

The particle size analysis of the samples was performed by a Dynamic Light Scattering (DLS) particle sizer (BI-90 Particle Size Analyser, Brookhaven Instrument Co.).

2.3.6. Morphology and homogeneity characterisation

The morphology and homogeneity of the synthesised materials were characterised by SEM (JEOL JSM-25SII and JEOL JSM-880). The EDS/SEM (Oxford Link GEM) was used for the

Table 1
The nomenclature list

#	Identification	Composition	Precipitation conditions	Calcination conditions
1.	CeO_2(lit)	CeO_2	Literature data [14]	
2.	$Ce_2(C_2O_4)_3$	$Ce_2(C_2O_4)_3$	Synthesised by ppt	Precursor
3.	CeO_2	CeO_2		400°C/2h in air
4.	CeO_2(a)	CeO_2		400°C/2h + 650°C/4h in air
5.	CeO_2(600/3)	CeO_2		600°C/3h in air
6.	Ce90Ca10(p)	$Ce_{0.9}Ca_{0.1}(C_2O_4)_{1.45}$	Synthesised by co-ppt in small volume	Precursor
7.	Ce90Ca10	$Ce_{0.9}Ca_{0.1}O_{2-\delta}$	synthesis reactor -i.e., beaker	600°C/3h in air
8.	Ce90Ca10(a)	$Ce_{0.9}Ca_{0.1}O_{2-\delta}$		600°C/3h + 650°C/4h in air
9.	Ce90Ca10Al50(p-seq-b)	$Ce_{0.9}Ca_{0.1}O_{2-\delta} \cdot 0.5Al_2O_3$	Synthesised by sequential co-ppt in beaker	Precursor
10.	Ce90Ca10Al50(seq-b)	$Ce_{0.9}Ca_{0.1}O_{2-\delta} \cdot 0.5Al_2O_3$		600°C/3h in air
11.	Ce90Ca10Al50(a-seq-b)	$Ce_{0.9}Ca_{0.1}O_{2-\delta} \cdot 0.5Al_2O_3$		600°C/3h + 650°C/4h in air
12.	Ce90Ca10Al50(p-sim-b)	$Ce_{0.9}Ca_{0.1}O_{2-\delta} \cdot 0.5Al_2O_3$	Synthesised by simultaneous co-ppt in	Precursor
13.	Ce90Ca10Al50(sim-b)	$Ce_{0.9}Ca_{0.1}O_{2-\delta} \cdot 0.5Al_2O_3$	beaker	600°C/3h in air
14.	Ce90Ca10Al50(a-sim-b)	$Ce_{0.9}Ca_{0.1}O_{2-\delta} \cdot 0.5Al_2O_3$		600°C/3h + 650°C/4h in air
15.	Ce90Ca10Al50(seq-r)	$Ce_{0.9}Ca_{0.1}O_{2-\delta} \cdot 0.5Al_2O_3$	Synthesised by sequential co-ppt in the	400°C/2h in air
16.	Ce90Ca10Al50(a-seq-r)	$Ce_{0.9}Ca_{0.1}O_{2-\delta} \cdot 0.5Al_2O_3$	large volume synthesis reactor	400°C/2h + 650°C/4h in air
17.	Ce63Zr37(comm)	$Ce_{0.63}Zr_{0.37}O_{2-\delta}$	Commercial	As received
18.	Ce63Zr37(comm-a)	$Ce_{0.63}Zr_{0.37}O_{2-\delta}$		calcined at 650°C/4h in air
19.	Ce80Zr20	$Ce_{0.8}Zr_{0.2}O_{2-\delta}$	Synthesised by co-ppt in the large volume	400°C/2h in air
20.	Ce80Zr20(a)	$Ce_{0.8}Zr_{0.2}O_{2-\delta}$	synthesis reactor	400°C/2h + 650°C/4h in air
21.	ZrO_2	ZrO_2	Commercial ZrO_2 powder	As received
22.	Ce80Zr20(ZrO_2)	$Ce_{0.8}Zr_{0.2}O_{2-\delta}$	Synthesised by ppt using commercial ZrO_2 in the large volume synthesis reactor	400°C/2h in air
23.	Ce80Zr20Al20	$Ce_{0.8}Zr_{0.2}O_{2-\delta} \cdot 0.2Al_2O_3$	Synthesised by sequential co-ppt in the	400°C/2h in air
24.	Ce80Zr20Al20(a)	$Ce_{0.8}Zr_{0.2}O_{2-\delta} \cdot 0.2Al_2O_3$	large volume synthesis reactor	400°C/2h + 650°C/4h in air
25.	Ce80Zr20Al40	$Ce_{0.8}Zr_{0.2}O_{2-\delta} \cdot 0.4Al_2O_3$	Synthesised by sequential co-ppt in the	400°C/2h in air
26.	Ce80Zr20Al40(a)	$Ce_{0.8}Zr_{0.2}O_{2-\delta} \cdot 0.4Al_2O_3$	large volume synthesis reactor	400°C/2h + 650°C/4h in air

The abbreviations – or combination of them – in parenthesis denote the followings: (lit) literature, (ppt) precipitation, (p) precursor, (sim) simultaneous, (seq) sequential, (a) aged, (comm) commercial, (b) small volume synthesis reactor, i.e. beaker, (r) large volume special synthesis reactor.

compositional analysis and for the distribution analysis of the doped cations. Moreover, Transmission Electron Microscopy (TEM) observations were carried out (Jeol 2000 EX Instrument). The TEM was equipped with a LINK probe LZ-5 EDSX detector for EDS spectroscopy analysis, as well. Samples were prepared by sonicating the nanophase powders in ethanol and dropping a small volume onto a carbon-coated copper grid.

Table 2
The pH values within which the precursor of each sample was (co-) precipitated

#	Precursor	pH range
2.	$Ce_2(C_2O_4)_3$	5.0-6.5
6.	Ce90Ca10(p)	6.0-7.0
9.	Ce90Ca10Al50(p-seq-b)	6.0-7.0 during the co-ppt of Ce-Ca particles ; 7.5-8.5 during the sequential ppt of Al(III)
12.	Ce90Ca10Al50(p-sim-b)	7.0-8.5
15.	Ce90Ca10Al50(seq-r)	6.0-7.0 during the co-ppt of Ce-Ca particles ; 7.5-8.5 during the sequential ppt of Al(III)
19.	Ce80Zr20	4.5-6.5
22.	Ce80Zr20(ZrO_2)	4.5-6.5
23.	Ce80Zr20Al20	5.0-7.5 during the co-ppt of Ce-Zr particles ; 7.5-8.5 during the sequential ppt of Al(III)
25.	Ce80Zr20Al40	5.0-7.5 during the co-ppt of Ce-Zr particles ; 7.5-8.5 during the sequential ppt of Al(III)

2.4. Oxygen storage capacity measurements

2.4.1. System set-up

The Temperature Programmed Reduction (TPR) set-up consists of digital mass flow meters, a quartz tube reactor in a tubular furnace, and a mass spectrometer. The sample was placed as a fixed bed above a layer of quartz wool in the tube reactor, while the temperature was measured directly above the sample. During each run, the evolved gases were analysed by a quadropole mass spectrometer (minilab LM80, Spectra) monitoring the partial pressure of water vapour.

2.4.2. Experimental procedure

Amount of 0.10 g of each sample was properly positioned inside the TPR reactor, after pelletising, crushing and sieving it to diameters between 0.075–0.500 mm. The samples were first oxidised into $Ce_{1-x}M_xO_2$ during heating up to 500°C with a heating rate of 20°C min^{-1} under a flowing gas mixture of 10 vol% O_2 and 90 vol% He at a total flow rate of 70 ml min^{-1}. Then, the sample was cooled down to room temperature under flowing He at 50 ml min^{-1}. Afterwards, a gas mixture of 15 vol% H_2 and 85 vol% He was introduced at a total flow rate of 70 ml min^{-1} into the system. After all the signals of the control system were stabilised at room temperature, the sample was heated up to 650 °C at 10 °C min^{-1} for its reduction into $Ce_{1-x}M_xO_{2-\delta}$. There, it remained for 1 min, and then cooled down to room temperature under flowing He at 50 ml min^{-1}.

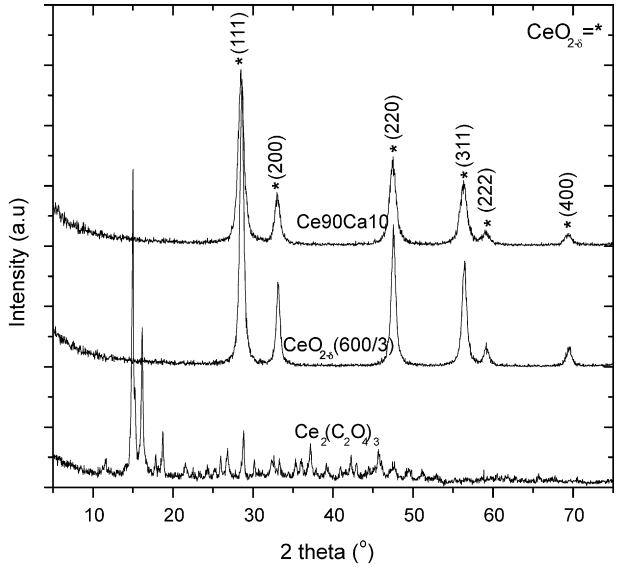

Fig. 2. The characteristic XRD profiles of precursor and calcined materials of the Ce/Ca system.

2.4.3. Data treatment

During a TPR measurement, both the temperature of the furnace and the thermocouple, which was placed just above the sample, were recorded. On the surface of the sample, hydrogen is combusted to produce water, which is a highly exothermic reaction. The ignition temperature (T_{ign}) is defined as the temperature when the thermocouple above the sample indicated that the exothermic reaction has set off, by showing a higher increasing rate for the temperature above the sample, compared to the increasing rate of the temperature, measured by the thermocouple located inside the furnace walls.

The peak area of each TPR profile was utilised to determine the OSC. This area was determined as the area below the peak of the TPR profile and a straight line, starting at the T_{ign} to end up at the next lowest temperature point of the profile. According to the literature,[27] pure CeO_2 can get reduced to $CeO_{1.833}$, while maintaining its fluorite structure in a form of CeO_2, so that the OSC is the maximum δ of 0.167 mol (atomic) O, that can be released/uptaken from 1 mol CeO_2. Herein, 0.097 mmol (atomic) O is released from 0.1 g (= 0.581 mmol) of pure CeO_2 during its reduction to reach its full OSC. The peak area of the OSC curve was 1.57E−6 (a.u.) for pure CeO_2 according to our TPR data. Thereby, the OSC of each $Ce_{1-x}Zr_xO_{2-\delta}{\cdot}yAl_2O_3$ sample (in mmol H_2 consumed/g catalyst) was calculated by correlating the respective peak area with that of pure CeO_2, known as the above (cf. Table 3).

Table 3
The OSC features of the synthesised nanostructured powders

#	Sample	OSC (H_2 mmole/g catalyst)	T_{ign} (°C)
3.	CeO_2	0.970	240
4.	CeO_2 (a)	0.914	240
7.	Ce90Ca10	1.144	180
8.	Ce90Ca10(a)	0.627	180
10.	Ce90Ca10Al50(seq-b)	0.906	210
11.	Ce90Ca10Al50(a-seq-b)	1.040	195
13.	Ce90Ca10Al50(sim-b)	1.063	170
14.	Ce90Ca10Al50(a-sim-b)	1.028	180
15.	Ce90Ca10Al50(seq-r)	0.924	200
17.	Ce63Zr37(comm)	0.717	235
18.	Ce63Zr37(comm-a)	0.455	285
19.	Ce80Zr20	1.162	190
20.	Ce80Zr20(a)	1.032	170
23.	Ce80Zr20Al20	1.019	230
24.	Ce80Zr20Al20(a)	0.766	170
25.	Ce80Zr20Al40	1.551	215
26.	Ce80Zr20Al40(a)	1.458	180

The TPR experiment was performed using 0.10 g of each sample.

3. Results and discussion

3.1. Powder characteristics

The materials included in the present study along with their OSC features and physicochemical properties are collected in Tables 1, 3 and 4, respectively. Crystallographic data along with the theoretical density ρ (ρ_{the}) data[28] of the oxides involved in the present study are given altogether in Table 5. In the present work, Zr(IV) and Ce(III) were precipitated as ZrO_2 and $Ce_2(C_2O_4)_3$, respectively, because the precipitation of $Zr_2(C_2O_4)_4$ was found difficult to be controlled due to its relatively high solubility.[20] Additionally, the sample Ce80Zr20 was also synthesised using ZrO_2 powder which served as seeds, on which Ce(III) precipitated as $Ce_2(C_2O_4)_3$, denoted herein as Ce80Zr20(ZrO_2).

In the case of $Ce_2(C_2O_4)_3$, the decomposition occurs between 300 and 350 °C, and therefore this sample was calcined at 400 °C for 2 h. In the case of the Ce90Ca10(p), the TGA analysis – not included herein – showed an additional weight drop at 580–600 °C which is likely attributed to the CaC_2O_4 decomposition. Therefore, this sample along with few others was calcined at 600 °C for 3 h. Besides, the XRD patterns of the precursors and the calcined oxides of CeO_2 and Ce80Zr20Al40, along with the aged material Ce80Zr20Al40 are presented in Fig. 3. As can be seen, the XRD pattern of the precursor Ce80Zr20Al40(p) shows

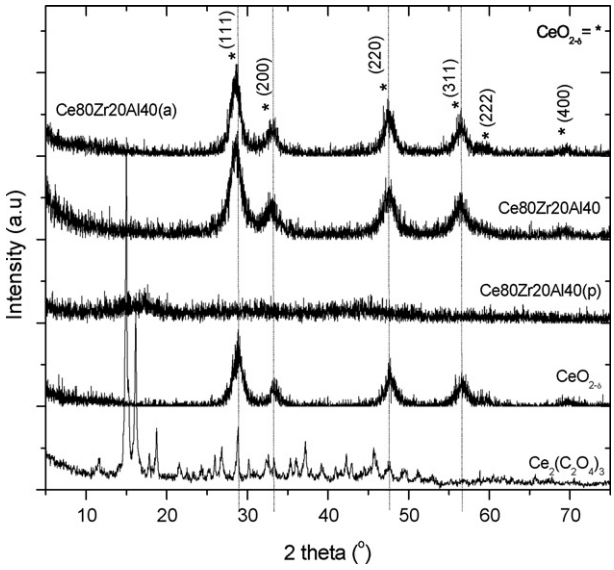

Fig. 3. The XRD patterns of the precursor and calcined $CeO_{2-\delta}$, the precursor, calcined and aged Ce80Zr20Al40 sample.

XRD-amorphous characteristics. After the heat-treatment, this powder became crystalline with the main characteristic CeO_2 peaks.

3.1.1. Particle size and morphology

In another study, it was reported that the (co-)precipitated precursor and calcined particles of CeO_2 had a shape of long-narrow plate-sheets,[3] which was also confirmed at the present one (cf. Fig. 4); the same also holds for the Al_2O_3-coated and uncoated $Ce_{1-x}Ca_xO_{2-\delta}$ particles (cf. Fig. 5). The decomposition of the oxalate precursor to its corresponding oxide – with the simultaneous release of carbon oxides gases – results in a dramatic decrease of the crystallite size, as determined by XRD, and a consequential increase of the surface area (cf. Table 4). In other words, during calcination the large particles of the precursors were broken down, as a result of the thermochemical decomposition of the metals-oxalate precipitated powder.

The morphology and microstructure of the synthesised particles were also studied by SEM and TEM, and showed the formation of primary, large agglomerates with average size in the order of 1 μm, which is in agreement with the data measured by the DLS particle sizer. Moreover in the case of doped samples, SEM backscattering investigation shows that the elements are homogeneously distributed through the individual particles, as the mapping of the samples Ce80Zr20 and Ce80Zr20Al20 reveal (cf. Fig. 6). The same observation holds for the rest of the $Ce_{1-x}Zr_xO_{2-\delta}$ samples.

3.1.2. Effect of doping

Comparing the physicochemical properties (cf. Table 4) of CeO_2 to Ce90Ca10 samples, both calcined at 600 °C for 3 h, it is evident that Ca-doping altered neither the specific surface area nor the density, but decreased its crystallite size (D_{XRD}) and had a little influence on the lattice parameter. According to the XRD patterns (cf. Fig. 3), most of the $Ce_{1-x}Zr_xO_{2-\delta}\cdot yAl_2O_3$ samples consist of a single phase, indicating that Zr was incorporated into

Table 4
The physicochemical properties of the synthesised materials presented herein

#	Composition	S_{BET} (m^2/g)	ρ (g/cm^3)	ρ_{the}* (g/cm^3)	D_{BET} (nm)	D_{XRD} (nm)	D_{DLS} (nm)	a_{XRD} (Å)
1.	CeO_2 (lit)	-	7.2	7.2	-	-	-	5.4120
2.	$Ce_2(C_2O_4)_3$	3	2.7	-	652	38	-	-
3.	CeO_2	104	6.3	7.3	9	8	715	5.3986
4.	CeO_2 (a)	19	-	7.5	-	20	-	5.3337
5.	CeO_2(600/3)	49	6.6	7.2	19	15	1200	5.4046
6.	Ce90Ca10(p)	5	2.6	-	480	-	-	-
7.	Ce90Ca10	49	6.6	6.8	19	11	-	5.4130
8.	Ce90Ca10(a)	38	-	6.8	-	-	-	-
9.	Ce90Ca10Al50(p-seq-b)	47	3.0	-	43	-	-	-
10.	Ce90Ca10Al50(seq-b)	78	4.9	5.9	16	14	2000	5.3948
11.	Ce90Ca10Al50(a-seq-b)	64	4.9	5.8	19	14	-	5.4078
12.	Ce90Ca10Al50(p-sim-b)	25	2.9	-	82	-	-	-
13.	Ce90Ca10Al50(sim-b)	35	4.2	5.8	41	16	1000	5.4063
14.	Ce90Ca10Al50(a-sim-b)	26	4.5	5.9	51	20	-	5.3889
15.	Ce90Ca10Al50(seq-r)	169	-	5.8	-	7	-	5.4147
16.	Ce90Ca10Al50(a-seq-r)	101	-	-	-	-	-	-
17.	Ce63Zr37(comm)	183	5.3	6.9	6	8	384	5.2861
18.	Ce63Zr37(comm-a)	61	-	6.9	-	8	-	5.2949
19.	Ce80Zr20	78	5.6	7.0	14	7	877	5.3707
20.	Ce80Zr20(a)	25	-	6.9	-	16	-	5.3996
21.	ZrO_2	84	5.3	5.8	13	13	-	-
22.	Ce80Zr20(ZrO_2)	65	-	6.8	-	8	1266	5.4071
23.	Ce80Zr20Al20	117	5.9	6.3	9	7	1007	5.4270
24.	Ce80Zr20Al20(a)	64	-	6.3	-	12	-	5.4138
25.	Ce80Zr20Al40	129	4.7	5.9	10	7	-	5.4237
26.	Ce80Zr20Al40(a)	82	7.8	6.0	9	6	-	5.4015

*The theoretical density (ρ_{the}) is calculated from the equation: $\rho_{the} = ZM_w/a^3N_A$, where 'α' is the cubic cell dimension of $Ce_{1-x}M_xO_{2-\delta}{\cdot}yAl_2O_3$ as determined by the XRD measurement.

Table 5
Summary of some crystallographic data of few oxides

Oxide	Z	M_w	α (Å)	b (Å)	c (Å)	β (°)	Crystallographic system	Cell volume ($\times 10^{-24}$ cm^{-3})	Density (g cm^{-3})
CeO_2	4	172.12	5.4110	–	–	–	Cubic	158.43	7.2150
CaO	4	56.08	4.8109	–	–	–	Cubic	111.34	3.3453
ZrO_2	4	123.22	5.1454	5.2075	5.3107	99.23	Monoclinic	140.46	5.8270
Al_2O_3	6	101.96	4.7591	–	12.9894	–	Hexagonal	254.78	3.9872

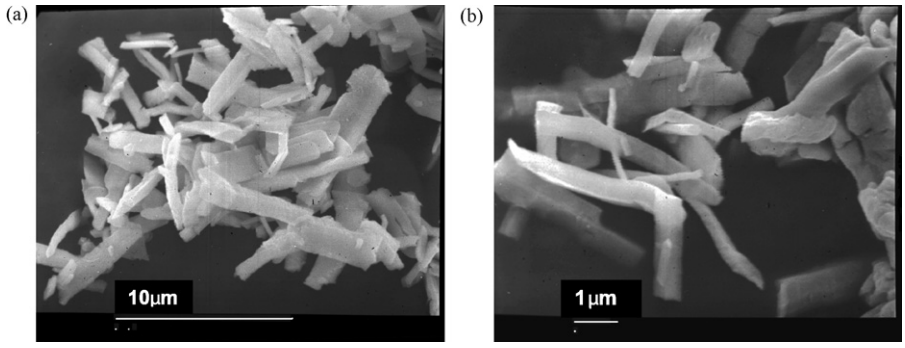

Fig. 4. SEM micrographs of the particles morphology of (a) $Ce_2(C_2O_4)_3$ and (b) $CeO_{2-\delta}$ calcined at 600 °C for 3 h. The bar with one and two dots below each micrograph denotes for 1 and 10 μm, respectively.

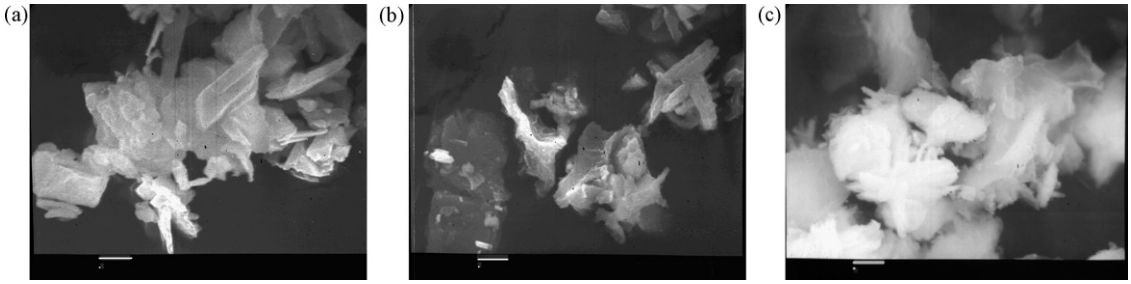

Fig. 5. SEM micrographs of the particles morphology of the samples Ce90Ca10(p) (a), Ce90Ca10Al50(p–seq–b) (b) and Ce90Ca10Al50(seq–b) (c). The bar with one dot below each micrograph denotes for 1 μ m.

the CeO_2 lattice forming solid solution. The retained fluorite structure of doped CeO_2 was slightly distorted, as revealed by their lattice parameters 'α' given in Table 4. On the other hand, the XRD pattern of the sample Ce80Zr20(ZrO_2), synthesised by precipitation of $Ce_2(C_2O_4)_3$ with ZrO_2 powder, did not only have a phase of CeO_2, but an additional phase of ZrO_2 as well (cf. Fig. 7). As shown in Table 4 and Fig. 8, Zr-doped CeO_2 maintained much higher specific surface area than the undoped one after aging, though it was the opposite before aging. This observation agrees also with the literature, which indicated that doping CeO_2 with Zr enhanced its thermal stability.[29–31]

3.1.3. *Effect of Al_2O_3-coating*

Regarding the Ce/Ca system, the specific surface area of the sequentially precipitated samples, no matter if it is a precursor, calcined or aged material, is more than double compared to that of the simultaneously co-precipitated sample, manifesting the effect of Al_2O_3-coating (cf. Table 4). Alumina seems to prevent the growth of the particles when heated at high temperature, by maintaining the CeO_2 particles separated from each other; thereby maintaining high specific surface area even after the heat treatment. This is also verified by the comparison of the S_{BET} of CeO_2 calcined at 600 °C for 3 h and Ce90Ca10, which is the same, whilst the S_{BET} was increased by 60% in the case of the sequential precipitation, i.e. Ce90Ca10Al50(seq–b). That can be a result of the high S_{BET} of Al_2O_3 itself and/or by the role of Al_2O_3-coating to prevent the growth of the Ce–Ca–oxalate particles.

As to the Ce/Zr system, the Al_2O_3-coating results in an increase of the specific surface area of the calcined materials; the higher the Al_2O_3-coating, the higher the specific surface area, as shown by the comparison of the calcined and aged samples Ce80Zr20, Ce80Zr20Al20 and Ce80Zr20Al40 (cf. Table 4 and Fig. 8). In particular, 20% and 40% Al_2O_3-coating over the Ce80Zr20 sample resulted in 50 and 65% further increase of the specific surface area, respectively. Furthermore, in the case of $Ce_{1-x}Zr_xO_{2-\delta}{\cdot}yAl_2O_3$ samples, no Al_2O_3 peak could be observed, probably because Al_2O_3 was X-ray amorphous. As to the crystal structure of both systems, Al_2O_3-coating does not seem to affect the phase formation of CeO_2, as shown from the XRD profiles of the Al_2O_3-coated samples (cf. Fig. 9 and Fig. 3).

3.1.4. *Effect of aging*

The effect of aging on the physicochemical properties is revealed by comparing the S_{BET} of CeO_2 calcined at 400 °C for 2 h, at 600 °C for 3 h and aged at 650 °C for 4 h (cf. Table 4). The S_{BET} of the CeO_2 samples calcined at 600 °C for 3 h and aged at 650 °C for 4 h decreased more than 50 and 80% respectively, compared to the one calcined at 400 °C for 2 h, due to the particles growth effect. Besides, aging results in a decrease of the S_{BET} due to particles growth, but this drop is restrained by the Al_2O_3-coating. For instance, the relative S_{BET} after aging of the Ce90Ca10 and Ce90Ca10Al(seq–b) samples decreased 22 and 18%, respectively. This significant effect of the Al_2O_3-coating on the S_{BET} of the calcined and the aged samples is also revealed in Fig. 10, where the specific surface area of calcined and aged materials of the Ce/Ca system is presented.

The XRD profiles of the calcined (cf. Fig. 9) and aged (cf. Fig. 11) Ce/Ca samples show that the thermal treatment

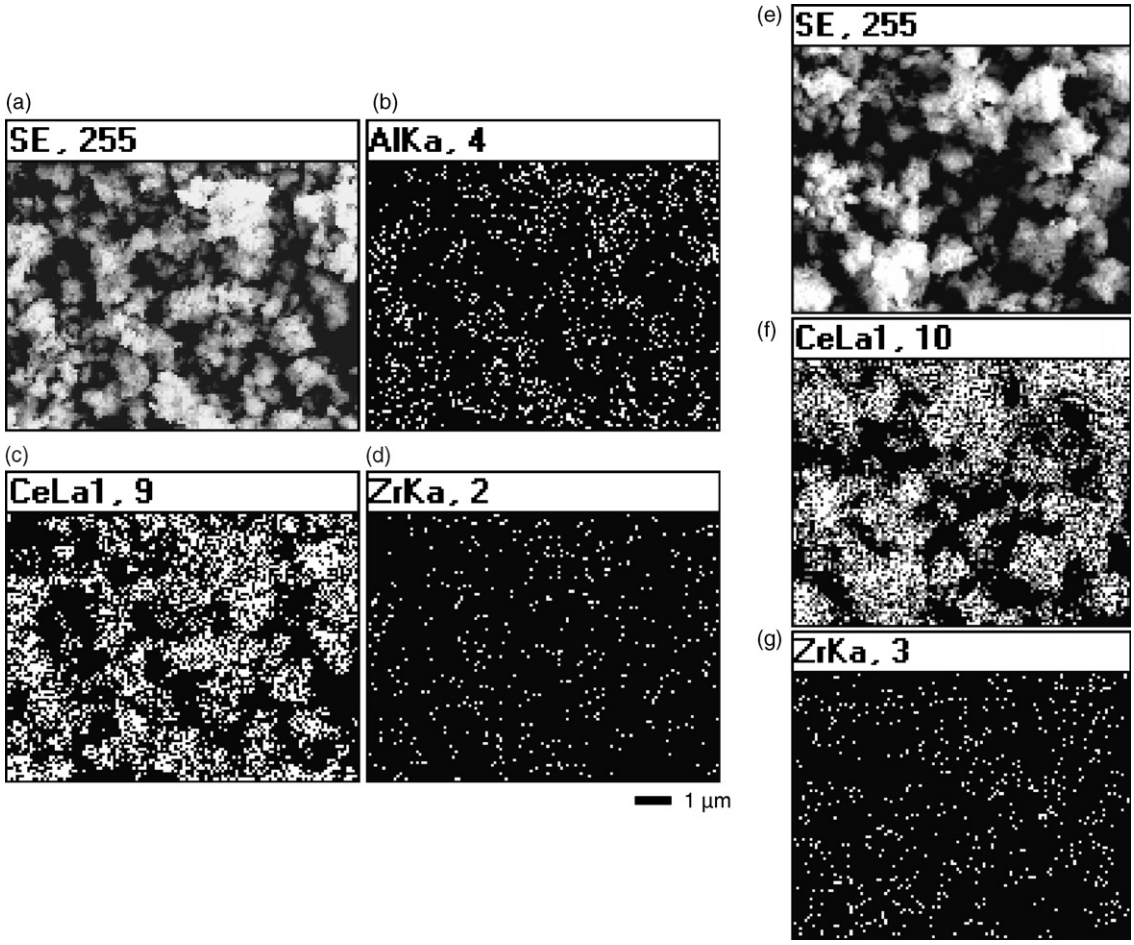

Fig. 6. Mapping of the Ce80Zr20 and Ce80Zr20Al20 samples calcined at 400 °C for 2 h in air. Fig. (a) and (e) show the micrograph of the overall particles area of the Ce80Zr20 and Ce80Zr20Al20 samples to be mapped, respectively. The Fig. (b), (c) and (d) show the elemental mapping of Al, Ce and Zr, respectively, for Ce80Zr20 sample. The Fig. (f) and (g) show the elemental mapping of Ce and Zr, respectively, for the Ce80Zr20Al20 sample. The elements are homogeneously distributed in the particles mass, as the micrographs reveal.

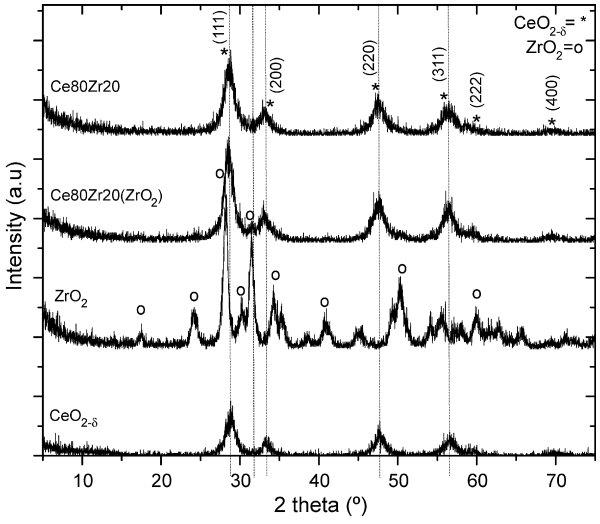

Fig. 7. The XRD patterns of the calcined $CeO_{2-\delta}$, ZrO_2, Ce80Zr20(ZrO_2) and Ce80Zr20. Note the extra peak of ZrO_2 at the pattern of the Ce80Zr20(ZrO_2) sample at 31.6°.

increases the crystallinity, as manifested by the narrowing and the increase of the XRD peak heights. The same holds for the samples of the Ce/Zr system, as their XRD patterns of the calcined and the aged samples reveal (cf. Fig. 3). Additionally, the aged samples consist of only a single phase, i.e. CeO_2, denoting that Ca or Zr is still incorporated inside the CeO_2 fluorite structure (cf. Figs. 11 and 3, respectively).

The specific surface area of pure CeO_2 decreases more than 80% after aging (cf. Table 4). This aging effect was reduced by Zr-doping, but not very remarkably, e.g. 67% for the Ce80Zr20(a) and the commercial Ce63Zr37(comm–a), though the latter exhibited the highest specific surface area before aging (cf. Fig. 8). However, the Al_2O_3-coating has shown a significant enhancement for the maintenance of the specific surface area after aging. After aging, the Ce80Zr20Al40(a) sample maintained 64% of its specific surface area, whilst Ce80Zr20(a), Ce63Zr37(comm–a) and CeO_2(a) did only 32, 33 and 18%, respectively. These results demonstrate that Al_2O_3-coating prevents the particles growth at the high temperature, maintaining the particles to separate from each other, and consequently hinder the decrease of the specific surface area.

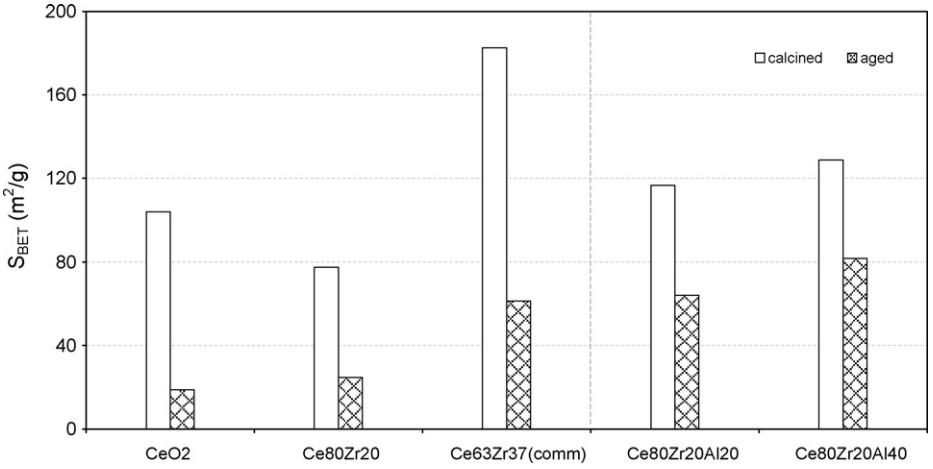

Fig. 8. The specific surface area of the calcined and aged synthesised materials of the Ce/Zr system.

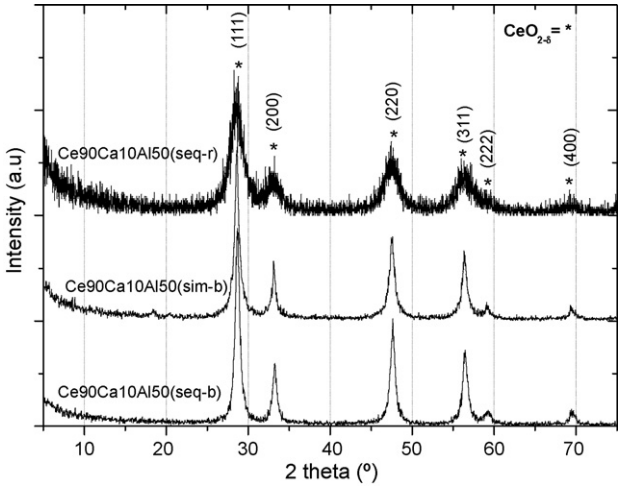

Fig. 9. Characteristic XRD profiles of a few calcined $Ce_{1-x}Ca_xO_{2-\delta}{\cdot}yAl_2O_3$ samples. The samples Ce90Ca10Al50(seq–b) and Ce90Ca10Al50(sim–b) were calcined at 600 °C for 3 h, while the Ce90Ca10Al50(seq–b) was calcined at 400 °C for 2 h. Note that no Al_2O_3 peaks appeared.

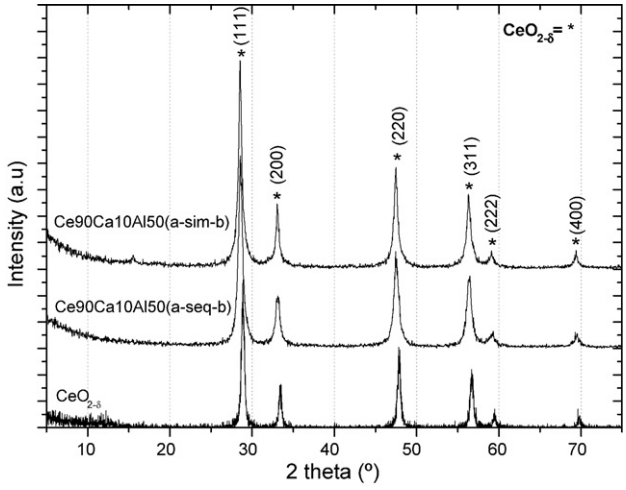

Fig. 11. Characteristic XRD patterns of few aged $Ce_{1-x}Ca_xO_{2-\delta}{\cdot}yAl_2O_3$ samples.

3.2. Oxygen storage capacity

3.2.1. Effect of doping

The doping of CeO_2 with Ca enhances its OSC (cf. Table 3 and Fig. 12), which is in agreement with earlier studies.[3] In particular, the sample Ce90Ca10 calcined at 600 °C for 3 h has higher OSC and lower T_{ign} than pure CeO_2, i.e. calcined at 400 °C for 2 h. The ionic radii of Ce(IV), Ce(III) and Ca(II) are 0.97, 1.143 and 1.12 Å[32], respectively, in their corresponding oxides with the same coordination number of O around Ce in CeO_2 lattice, i.e. 8. That is to say, these metal cations are

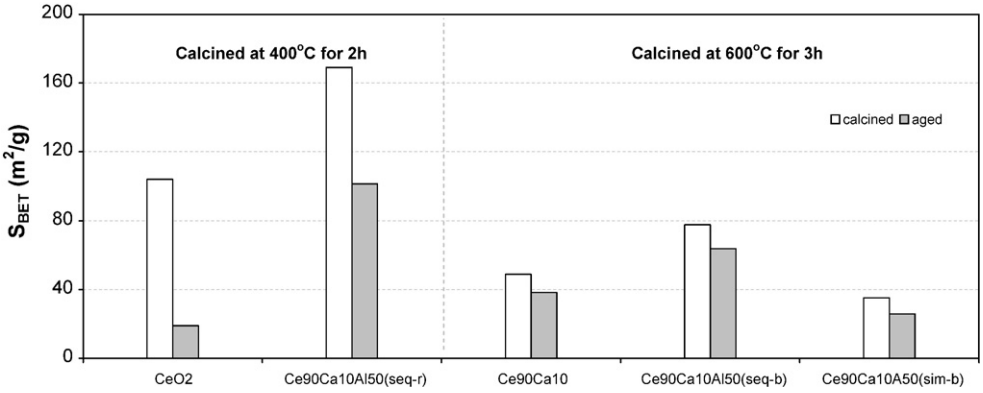

Fig. 10. The S_{BET} of several calcined and aged $Ce_{1-x}Ca_xO_{2-\delta}{\cdot}yAl_2O_3$ samples.

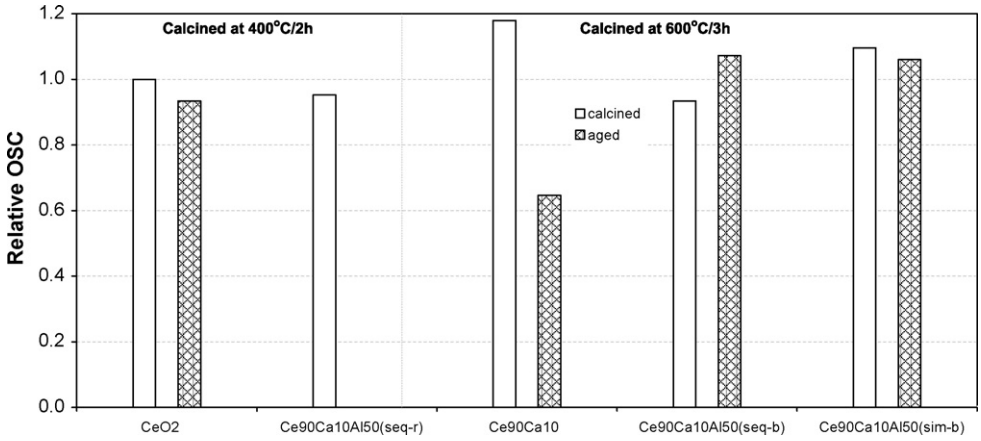

Fig. 12. Histograms showing the ratios [OSC $Ce_{1-x}Ca_xO_{2-\delta}{\cdot}yAl_2O_3$/OSC $CeO_{2-\delta}$] and [OSC $Ce_{1-x}Ca_xO_{2-\delta}{\cdot}yAl_2O_3$(a)/OSC $CeO_{2-\delta}$].

expected to be miscible in CeO_2 lattice and can be the substitution for Ce(IV) cations. That was also confirmed by the XRD data (cf. Fig. 2 and Fig. 9), which indicated the formation of a single phase of CeO_2. The Ca-doping of CeO_2 results in the formation of a non-stoichiometric compound containing oxygen vacancies and structural defects; the OSC enhancement is likely attributed to these vacancies and defects (cf. Table 3).

When introducing Zr to the CeO_2 lattice, the OSC is enhanced as shown in Table 3 and Fig. 13, where the relative OSC of the calcined and aged $Ce_{1-x}Zr_xO_{2-\delta}{\cdot}yAl_2O_3$ samples compared with that of CeO_2 are presented, i.e. the ratios [OSC of $Ce_{1-x}Zr_xO_{2-\delta}{\cdot}yAl_2O_3$]/[OSC of CeO_2] and [OSC of $Ce_{1-x}Zr_xO_{2-\delta}{\cdot}yAl_2O_3$(a)]/[OSC of CeO_2]. Doping CeO_2 with Zr results in a decrease of the T_{ign}, and the synthesised by co-precipitation samples showed better OSC features compared to the commercial one. The commercial sample showed a much lower OSC, though it had a higher percentage of Zr-doping.

3.2.2. *Effect of Al_2O_3-coating*

The effect of Al_2O_3-coating through the subsequent precipitation of Al(III) on the preformed precursor has been studied. The sequential precipitation of $Al(OH)_3$ results in the formation of materials with higher T_{ign} and 15% lower OSC compared to the simultaneous one—compare the OSC of Ce90Ca10Al50(seq–b) to Ce90Ca10Al50(sim–b) (cf. Table 3). A likely explanation is that during the sequential precipitation, more active sites are covered by $Al(OH)_3$, resulting in a lower catalytic activity. As can be noticed from Fig. 12, Ca-doping in CeO_2 – i.e. Ce90Ca10 sample – improves the OSC, which decreases 55% after aging. However, after the Al_2O_3-coating the OSC of the Ce90Ca10Al50(seq–b) sample is at the same level before and after aging.

The Al_2O_3-coating over the Ce80Zr20 particles affected the OSC and increased the T_{ign}. In particular, comparing the OSC of Ce80Zr20 and Ce80Zr20Al20 samples, it is shown that addition of Al_2O_3-coating decreases the OSC by 12%, and increases T_{ign} from 190 to 230 °C (cf. Table 3). However, the addition of more Al_2O_3 (Ce80Zr20Al40 sample) increases the OSC by 34% and T_{ign} from 190 to 215 °C.

3.2.3. *Effect of aging*

In the case of the Ce/Ca system, the T_{ign} of almost all samples decreases after aging (cf. Table 3). The lower T_{ign}, the better, since $Ce_{1-x}Ca_xO_{2-\delta}{\cdot}yAl_2O_3$ can buffer oxygen at lower

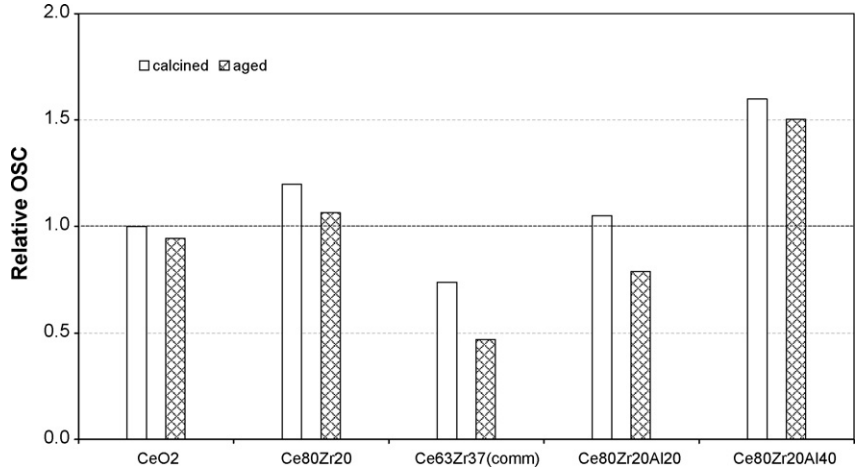

Fig. 13. The effect of doping of CeO_2 on its OSC is demonstrated by the ratios [OSC of $Ce_{1-x}Zr_xO_{2-\delta}{\cdot}yAl_2O_3$]/[OSC of $CeO_{2-\delta}$] and [OSC of $Ce_{1-x}Zr_xO_{2-\delta}{\cdot}yAl_2O_3$(a)]/[OSC of $CeO_{2-\delta}$, where $CeO_{2-\delta}$ has been synthesised by ppt and calcined at 400 °C for 2 h.

temperature. In that case, the amount of the produced toxic gases can be treated at lower temperatures. The aging results in decrease of the OSC and T_{ign} of all samples of the Ce/Zr system, whether or not coated with Al_2O_3 that were synthesised by co-precipitation (cf. Table 3). However, the T_{ign} of the Ce63Zr37(comm) increased after aging, whilst that of CeO_2 did not alter at all. This decrease in OSC can be attributed to the particles growth during the aging, resulting in the subsequent decrease of the specific surface area of the samples. Interestingly, the fresh and aged commercial materials Ce63Zr37(comm) and Ce63Zr37(comm–a) have the lowest OSC. Decrease of the crystallite size results in an increase of the OSC of the samples synthesised by co-precipitation (cf. Tables 3 and 4). This occurs due to the increase of the active sites of $Ce_{1-x}Zr_xO_{2-\delta}$ when the crystallite size decreases and consequently the specific surface area increases.

After aging, the OSC of CeO_2, Ce80Zr20, Ce80Zr20Al20 and Ce80Zr20Al40 samples decreased 6, 11, 25 and 6%, respectively. Nevertheless, compared to that of CeO_2(a) sample, the OSC of the last three aged samples is +12%, −16% and +60% higher. The Ce80Zr20Al40 sample showed the highest OSC after aging (cf. Fig. 13). On the other hand, T_{ign} of these samples decreased after aging.

4. Conclusions

A novel method for the synthesis of nanosized Al_2O_3-coated $Ce_{1-x}M_xO_{2-\delta}$ (M = Zr or Ca) has been developed. It is based on a sequential co-precipitation under controlled chemical and hydrodynamic conditions, resulting in oxides with a crystallite size on the order of 10 nm. The doping of CeO_2 enhanced its OSC, while the simultaneous Al_2O_3-coating restrained the particles growth. Thereby, its thermal stability was improved with respect to the specific surface area and the OSC upon aging.

Acknowledgements

The work has been financially supported by ‘Umicore AG & Co. KG’. The authors would like to thank Dr. Anke Wolf, ‘Umicore AG & Co. KG’, for fruitful discussions.

References

1. Schmid, G., *Nanoparticles: From Theory to Application*. Wiley VCH, Weinheim, Germany, 2004, pp. 1–3.
2. Ozin, G. A. and Arsenault, A. C., *Nanochemistry: A Chemical Approach to Nanomaterials*. The Royal Society of Chemistry, Cambridge, UK, 2005, pp. 1–45.
3. Zhang, Y., Andersson, S. and Muhammed, M., Nanophase catalytic oxides. I. Synthesis of doped cerium oxides as oxygen storage promoters. *Appl. Catal. B: Environ.*, 1995, **6**(4), 325–337.
4. Trovarelli, A., Leitenburg, C de. and Dolcetti, G., Design better ceria-based oxidation catalysts. *Chem. Technol.*, 1997, **27**(6), 32–37.
5. Fisher, G. B., Thesis, J. R., Casarella, M. V. and Mahan, S. T., The role of ceria in automotive exhaust catalysis and OBD-II catalyst monitoring. SAE paper 931034, 1993.
6. Harper, C. A., *Handbook of Ceramics, Glasses, and Diamonds, Technology Seminars, Inc.*. Mc-Graw Hill, Lutherville, MD, 2001, pp. 1.15.
7. *Materials Handbook: Ceramic industry*. Corcoran Communications, Solon, OH, USA, 1989, p. 21.
8. Chopin, T., Touret, O. and Vilmin, G., Thermally stable/highly reducible catalyst compositions comprising alumina and the oxides of cerium and zirconium. US Patent 5.883.037, 1999.
9. de Leitenburg, C., Trovarelli, A., Liorca, J., Cavani, F. and Bini, G., The effect of doping CeO_2 with zirconium in the oxidation of isobutane. *Appl. Catal. A: Gen.*, 1996, **139**(1), 161–173.
10. Hori, A. E., Permana, H., Simon Ng, K. Y., Brenner, A., More, K., Rahmoeller, K. M. and Belton, D., Thermal stability of oxygen storage properties in a mixed CeO_2–ZrO_2 system. *Appl. Catal. B: Environ.*, 1998, **16**, 105–117.
11. Fornasiero, P., Di Monti, R., Ranga Rao, G., Kaspar, J., Meriani, S., Trovarelli, A. and Graziani, M., Rh-loaded CeO_2–ZrO_2 solid-solutions as highly efficient oxygen exchangers: dependence of the reduction behavior and the oxygen storage capacity on the structural properties. *J. Catal.*, 1995, **151**, 168–177.
12. Trovarelli, A., Zamar, F., Llorca, J., de Leitenburg, C., Dolcetti, G. and Kissz, J., Nanophase fluorite-structured CeO_2–ZrO_2 catalysts prepared by high-energy mechanical milling: analysis of low-temperature redox activity and oxygen storage capacity. *J. Catal.*, 1997, **169**, 490–502.
13. Fornasiero, P., Balducci, G., Di Monte, R., Kaspar, J., Sergo, V., Gubitosa, G., Ferrero, A. and Graziani, M., Modification of the redox behaviour of CeO_2 induced by structural doping with ZrO_2. *J. Catal.*, 1996, **164**, 173–183.
14. de Carolis, S., Pascual, J. L., Pettersson, L. G. M., Baudin, M., Wojcik, M., Hermansson, K., Palmqvist, A. E. C. and Muhammed, M., ‘Structure and electronic properties of Ca-doped CeO_2 and implications on catalytic activity: an experimental and theoretical study. *J. Phys. Chem. B*, 1999, **103**(36), 7627–7636.
15. Turkki, T., Studies on preparation and properties of nanophase metal oxides. PhD Thesis. The Royal Institute of Technology, Stockholm, Sweden, 1999, ISBN 91-7170-411-6.
16. Ozawa, M., Kimura, M. and Isogai, A., The application of Ce–Zr oxide solid solution to oxygen storage promoters in automotive catalysts. *J. Alloys Comp.*, 1993, **193**, 73–75.
17. Yahiro, H., Ohuchi, T., Eguchi, K. and Arai, H., Electrical properties and microstructure in the system ceria-alkaline earth oxide. *J. Mater. Sci.*, 1988, **23**, 1036–1041.
18. Suzuki, T. and Sobukawa, H., Composite oxide, composite oxide carrier and catalyst. US Patent 6.306.794, 2001.
19. Suzuki, T. and Sobukawa, Composite oxide, composite oxide carrier and catalyst. US Patent 6.150.288, 2000.
20. Agrafiotis, C., Tsetsekou, A., Stournaras, S. J., Julbe, A., Dalmazio, L. and Guizard, C., Deposition of nanophase doped-ceria systems on ceramic honeycombs for automotive catalytic applications. *Solid State Ionics*, 2000, **136**, 1301–1306.
21. Muhammed, M., Adamopoulos, O., Bog, T., Mussmann, L., Lindner, D., Votsmeier, M., Feger, M., Lox, E. and Kreuzer, T., Oxygen storage material, process for its preparation and its application in a catalyst. US Patent 20060052243.
22. Puigdomenech, I., *INPUT, SED and PREDOM: Computer Programs Drawing Equilibrium Diagrams*, Report TRITA-OOK-3010. The Royal Institute of Technology, Stockholm/Sweden.
23. Persson, A. E., Zhang, Y. and Muhammed, M., Catalyst materials for high temperature processes. *Ceramic Transactions*, *vol. 73*. American Ceramic Society, Westerville, OH, 1997, p. 85.
24. Zhang, Y., Fang, Z., Muhammed, M., Rao, K. V., Skumryev, V., Medelius, H. and Costa, J. L., The synthesis of superconducting bismuth compounds via oxalate coprecipitation. *Physica C*, 1989, **157**(1), 108–114.
25. Klug, H. P. and Alexander, L. E., *X-ray Diffraction Procedure*. John Wiley & Sons, Inc., New York, 1954, p. 491.
26. Cullity, B. D., *Elements of X-ray Diffraction* (*2nd ed.*). Addison–Wesley, 1978, p. 285.
27. Trovarelli, A., *Catalysis by Ceria and Related Materials, Catalytic Science Series*, *vol. 2*. World Scientific Publishing Company, 2002, p. 16.
28. Weast, R. C. and Astle, M. J., *CRC Handbook of Chemistry and Physics*. CRC Press Inc., 1980, p. B196.

29. Kašpar, J., Fornasiero, P. and Graziani, M., Use of CeO_2-based oxides in the three-way catalysis. *Catal. Today*, 1999, **50**(2), 285–298.
30. Fornasiero, P., Balducci, G., Di Monte, R., Kašpar, J., Sergo, V., Gubitosa, G., Ferrero, A. and Graziani, M., Modification of the redox behaviour of CeO_2 induced by structural doping with ZrO_2. *J. Catal.*, 1996, **164**, 173–183.
31. Yashima, M., Arashi, H., Kakihana, M. and Yoshimura, M., Raman scattering study of cubic–tetragonal phase transition in $Zr_{1-x}Ce_xO_2$ solid solution. *J. Am. Ceram. Soc.*, 1994, **77**, 1067–1071.
32. Shannon, R. D., Revised effective ionic radii and systematic studies of interatomic distances in halides and chalcogenides. *Acta Crystallogr.*, 1976, **A32**, 751–767.